JCTC Journal of Chemical Theory and Computation

Article

pubs.acs.org/JCTC

Ab Initio Molecular Dynamics Using Recursive, Spatially Separated, Overlapping Model Subsystems Mixed within an ONIOM-Based Fragmentation Energy Extrapolation Technique

Junjie Li and Srinivasan S. Iyengar*

Department of Chemistry and Department of Physics, Indiana University, 800 E. Kirkwood Ave, Bloomington, Indiana 47405, United States

Supporting Information

ABSTRACT: Here, we demonstrate the application of fragment-based electronic structure calculations in (a) *ab initio* molecular dynamics (AIMD) and (b) reduced dimensional potential calculations, for medium- and large-sized protonated water clusters. The specific fragmentation algorithm used here is derived from ONIOM, but includes multiple, overlapping "model" systems. The interaction between the various overlapping model systems is (a) approximated by invoking the principle of inclusion-exclusion at the chosen higher level of theory and (b) within a real calculation performed at the chosen lower level of theory. The fragmentation algorithm itself is written using bit-manipulation arithmetic, which will prove to be advantageous, since the number of fragments in such methods has the propensity to grow exponentially with system size. Benchmark calculations are performed for three different protonated water clusters: $H_9O_4^+$, $H_{13}O_6^+$ and $H(H_2O)_{21}^+$. For potential energy surface benchmarks, we sample the normal coordinates and compare our surface energies with full MP2 and CCSD(T) calculations. The mean absolute error for the fragment-based algorithm is <0.05 kcal/mol, when compared with MP2 calculations, and <0.07 kcal/mol, when compared with CCSD(T) calculations over 693 different geometries for the $H_9O_4^+$ system. For the larger $H(H_2O)_{21}^+$ water cluster, the mean absolute error is on the order of a 0.1 kcal/mol, when compared with full MP2 calculations for 84 different geometries, at a fraction of the computational cost. *Ab initio* dynamics calculations were performed for $H_9O_4^+$ and $H_{13}O_6^+$, and the energy conservation was found to be of the order of 0.01 kcal/mol for short trajectories (on the order of a picosecond). The trajectories were kept short because our algorithm does not currently include dynamical fragmentation, which will be considered in future publications. Nevertheless, the velocity autocorrelation functions and their Fourier transforms computed from the fragment-based AIMD approaches were found to be in excellent agreement with those computed using the respective higher level of theory from the chosen hybrid calculation.

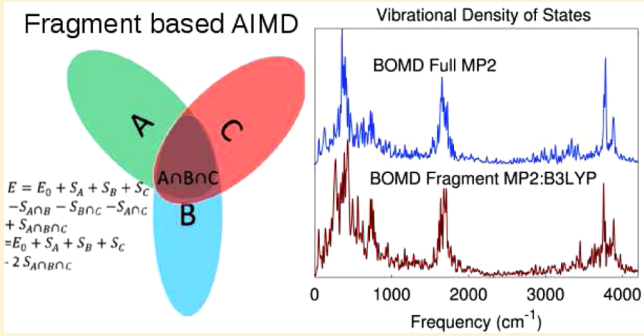

I. INTRODUCTION

Accurate prediction of molecular properties such as energy, structure, spectra, and those arising from dynamics and appropriate sampling of potential surfaces beyond the harmonic approximation, for large-sized systems, such as peptides, water clusters, and biological and atmospheric reactive intermediates is a grand challenge for computational chemistry. Despite the great advances in correlated electronic structure methods[1−3] and density functional theory (DFT),[4] the intrinsic scaling ($O(N^4)$ for DFT with hybrid functionals, $O(N^5)$ for MP2, and $O(N^6)$ for CCSD(T)) restricts the system size involved during "on-the-fly" classical[5−8] and quantum nuclear dynamics[9−15] that utilize *ab initio* potentials. For these reasons, hybrid quantum mechanics/molecular mechanics (QM/MM) methods[16−34] were developed where a large molecule is partitioned into multiple layers with each layer treated at different levels of theory. In recent years, molecular fragmentation methods[35−53] have emerged as powerful alternatives to address the computational scaling problem highlighted above. In this class of methods, a molecule or cluster is divided into fragments and the total energy of the system is assembled from the energy of individual pieces, along with suitably chosen interaction terms. Details of these methods can be found in several recently published articles and reviews.[35,41,50,54,55]

While a variety of QM/MM schemes have been used for both static electronic structure calculations,[23,33,35,41,50,54,55] *ab initio* molecular dynamics (AIMD) calculations[56−60] and quantum wavepacket dynamics calculations,[11] some of which facilitate rare, reactive events,[57,58,61,62] the study of fragmentation methods has been mainly focused on static calculations. Notable exceptions include the work of Li and co-workers,[49] who studied the dynamics of a model peptide using their Generalized Energy Based Fragmentation (GEBF) method, and the work of Gordon and co-workers,[63−66] who developed analytical gradients for the

Received: May 11, 2015
Published: August 7, 2015

DOI: 10.1021/acs.jctc.5b00433
J. Chem. Theory Comput. 2015, 11, 3978−3991

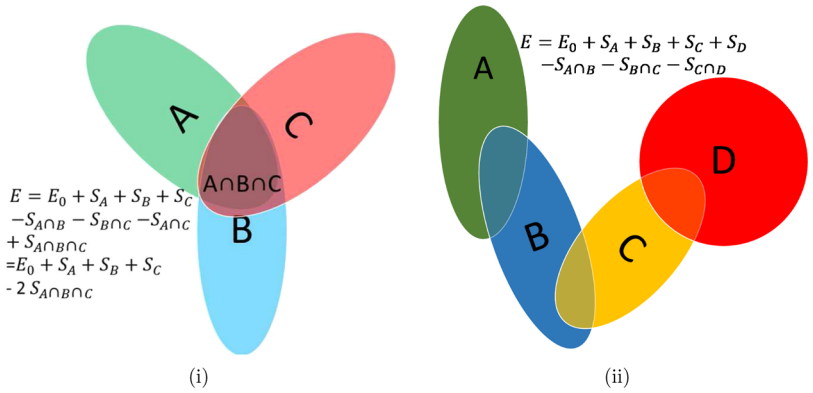

Figure 1. A simple illustration for the energy expression in eq 2. In panel (i), the three primitive fragments share only one common region; hence, there is only one derivative fragment constructed. Thus, $-S_{A\cap B} - S_{B\cap C} - S_{A\cap C} + S_{A\cap B\cap C}$ terms are simplified to be $-2S_{A\cap B\cap C}$. In panel (ii), the intersections between primitive fragments are all different and three derivative fragments are necessary.

fragment molecular orbital (FMO) method to construct classical trajectories for liquid water, water clusters,[66] and model peptides.

Here, we further explore the application of a fragment-based electronic structure methodology, including mechanical as well as electronic embedding, to AIMD, and we subsequently compute reduced dimensional potential energy surfaces (PES) to gauge quantum nuclear effects. Our benchmark systems include moderately sized protonated water clusters. We have also computed dynamically averaged vibrational properties using our classical nuclear trajectories obtained from AIMD. Future publications will probe the utility of these energy partitioning schemes for quantum dynamics, and treat larger-sized biological systems, where dynamical hydrogen-bonds may have a critical role. In the current publication, the energetic and dynamical properties are benchmarked against regular calculations that do not use the fragmentation scheme. The paper is thus organized as follows. Section II contains the theoretical aspects of the fragmentation technique employed here. When appropriate, our technique is contrasted with other well-known fragmentation algorithms. In Section III, we present the results. Specifically, Subsection III(B) includes a discussion on the potential energy surfaces obtained for $H_9O_4^+$ and $H(H_2O)_{21}^+$, and Subsection III(C) details AIMD studies on $H_9O_4^+$ and $H_{13}O_6^+$. Finally, conclusions are given in Section IV.

II. SPATIALLY SEPARATED, OVERLAPPING MODEL SUBSYSTEMS MIXED WITHIN AN ONIOM-BASED ENERGY PARTITIONING SCHEME

In most of the recent methods,[36,37,42,43,45,49,51,52] fragments are allowed to overlap. To avoid ambiguity, in a manner consistent with the works of Raghavachari and Saha[41] and Collins and Bettens,[50] in this paper, the overlapping unit is termed "derivative fragment", while the original fragments are called "primitive fragments". The word "fragment" here refers to either type. The common feature among all fragmentation methods is that energies from all primitive fragments are additive. Furthermore, the overcounted regions form derivative fragments that are then subtracted with proper coefficients in a manner consistent with the well-known Principle of Inclusion and Exclusion (PIE), from set theory:[67]

$$|\bigcup_{i=1}^{n} A_i| = \sum_{i=1}^{n} |A_i| - \sum_{1\le i<j\le n} |A_i \cap A_j| + \sum_{1\le i<j<k\le n} |A_i \cap A_j \cap A_k| - \cdots + (-1)^{n-1}|A_1 \cap \cdots \cap A_n| \quad (1)$$

To introduce interactions between nonoverlapping fragments, in a manner consistent with the ONIOM procedure,[23] we add additional layers over and above the PIE fragmentation expression above, such that the overall molecular energy becomes

$$E \approx E^{level,0}(0) + \sum_{i=1}^{n} \mathcal{S}(i) - \sum_{1\le i<j\le n} \mathcal{S}(i\cap j) + \sum_{1\le i<j<k\le n} \mathcal{S}(i\cap j\cap k) - \cdots + (-1)^{n-1} \sum \mathcal{S}(1\cap\cdots\cap n) \quad (2)$$

The terms $\mathcal{S}(i)$, $\mathcal{S}(i\cap j)$, $\mathcal{S}(i\cap j\cap k)$, etc., represent a correction to the energy of primitive and derivative fragments (i), $(i\cap j)$, $(i\cap j\cap k)$, etc., the latter being formed from the intersection of primitive fragments. At the simplest approximation (employed in this publication), the extrapolation is a correction term for the total energy from a lower level of theory, $[level,0]$, toward a higher level, $[level,1]$, according to

$$\mathcal{S}(i) = E^{level,1}(i) - E^{level,0}(i) \quad (3)$$

However, more sophisticated approximations to $\mathcal{S}(i)$, $\mathcal{S}(i\cap j)$, $\mathcal{S}(i\cap j\cap k)$, etc. are possible. The term $\mathcal{S}(i)$ may reflect a recursive extrapolation wherein additional partitioning of the fragment may be enforced. These partitioning schemes may themselves be akin to that employed in eq 2. Thus, in eq 4 below, the correction is recursively extrapolated through η subfragments within i. The α_ith sub-fragment or layer is a subset of atoms within the fragment i that is treated at two levels of theory, namely, $[level, \alpha_i]$ and $[level, \alpha_i + 1]$:

$$\mathcal{S}(i) = \sum_{\alpha_i=0}^{\eta} \left(E^{level,\alpha_i+1}_{\text{recursive-fragment},\alpha_i}(i) - E^{level,\alpha_i}_{\text{recursive-fragment},\alpha_i}(i) \right) \quad (4)$$

While each fragment or subfragment is treated at two levels of theory (α_i and $\alpha_i - 1$), the entire system is only considered at the lowest level of theory ($E^{level,0}(0)$).

If chemical bonds intersect the boundary between two layers, link atoms are used to saturate the dangling valencies of the smaller system.[68] The positions of link atoms are uniquely determined based on the connectivity of the system.[68] Thus, the selected atoms and additional link atoms of each system are influenced by the properties of the atoms in the larger systems.

DOI: 10.1021/acs.jctc.5b00433
J. Chem. Theory Comput. 2015, 11, 3978−3991

The expressions above are a simple extension of the standard ONIOM formalism, obtained by incorporating the inclusion-exclusion principle. Two pictorial illustrations for this scheme are provided in Figure 1. It is is instructive to rewrite the overall energy expressions for the two illustrations provided in Figure 1. Using eq 3 and the expressions given in Figure 1, we obtain the following:

Figure 1(i):

$$\begin{aligned} E = {} & [E^1(A) + E^1(B) + E^1(C)] - \\ & [E^1(A \cap B) + E^1(A \cap C) + E^1(B \cap C) - E^1(A \cap B \cap C)] + \\ & E^0 - [E^0(A) + E^0(B) + E^0(C)] + \\ & [E^0(A \cap B) + E^0(A \cap C) + E^0(B \cap C) - E^0(A \cap B \cap C)] \end{aligned} \tag{5}$$

where, for the sake of brevity, we have substituted $\{level,0 \rightarrow 0\}$ and $\{level,1 \rightarrow 1\}$ and rearranged the energy expression to clarify interaction between fragments. For example, the first line in eq 5 includes the total noninteracting fragment energy at *level*,1 and the second line then accounts for overcounting in *level*,1. The third and fourth lines in eq 5 account for the interaction energy between the various fragments at *level*,0, along with the remaining terms required to remove overcounting. Similarly, the energy expression for the partitioning shown in Figure 1(ii) may be expressed as follows:

Figure 1(ii):

$$\begin{aligned} E = {} & [E^1(A) + E^1(B) + E^1(C) + E^1(D)] - \\ & [E^1(A \cap B) + E^1(B \cap C) + E^1(C \cap D)] + \\ & E^0 - [E^0(A) + E^0(B) + E^0(C) + E^0(D)] + \\ & [E^0(A \cap B) + E^0(B \cap C) + E^0(C \cap D)] \end{aligned} \tag{6}$$

These expressions show that all interactions between fragments are captured at *level*,0. While this is true for the implementation of the extrapolation term given in eq 3, the term in eq 4 provides a more adaptive and tailored interaction scheme where sub-fragments represented within eq 4 may interact at levels higher than *level*,0. An implementation of the expression in eq 4, along with a detailed discussion of the associated benefits of this recursive partitioning, will be probed in future publications.

Further note that if only a single fragment and two levels of theory are used, eqs 2 and 3 reduce to

$$E \approx E^L(0) + E^H(1) - E^L(1) \tag{7}$$

which is exactly the energy expression in the popular two-layer ONIOM scheme. Although the formalism above is essentially derived from ONIOM, it also has close connections to the molecules-in-molecules (MIM) methodology,[42] the molecular tailoring approach,[37] and connectivity-based hierarchy (CBH)[69] ideas.

Similar to conventional QM/MM approaches,[54,55,70,71] eqs 2−4 may be augmented by introducing electronic embedding, and, in this case, charges from the immediate lowest level calculation serve as background charges for the fragment calculations. Here, Mulliken charges from the lower level are used for electronic embedding, and other types of charges will be studied in future publications.

In this formalism, the overlap between all primitive fragments must be evaluated (a simple bit manipulation algorithm is provided in Appendix A for this purpose). While the formalism above is presented for an arbitrary number of levels of theory, all applications presented here include two levels of theory.

II(A). Gradients. As in standard AIMD, eq 2 can be differentiated with respect to all variables that contribute to the energy expression, such as the real coordinates of the system. The gradients in this case are

$$\begin{aligned} \frac{\partial E}{\partial \mathbf{R}} \approx {} & \frac{\partial E^L(0)}{\partial \mathbf{R}} + \sum_{i=1}^{n} \frac{\partial \mathcal{S}(i)}{\partial \mathbf{R}} - \sum_{1 \le i < j \le n} \frac{\partial \mathcal{S}(i \cap j)}{\partial \mathbf{R}} + \\ & \sum_{1 \le i < j < k \le n} \frac{\partial \mathcal{S}(i \cap j \cap k)}{\partial \mathbf{R}} \cdots + (-1)^{n-1} \frac{\partial \mathcal{S}(1 \cap \cdots \cap n)}{\partial \mathbf{R}} \end{aligned} \tag{8}$$

where $\partial \mathcal{S}(i)/\partial \mathbf{R}$ is simply the gradient for each term in the correction

$$\frac{\partial \mathcal{S}(i)}{\partial \mathbf{R}} = \left(\frac{\partial E^{level,1}(i)}{\partial \mathbf{R}_i} - \frac{\partial E^{level,0}(i)}{\partial \mathbf{R}_i} \right) \frac{\partial \mathbf{R}_i}{\partial \mathbf{R}} \tag{9}$$

or the recursive extrapolation term,

$$\frac{\partial \mathcal{S}(i)}{\partial \mathbf{R}} = \sum_{\alpha_i=0}^{\eta} \left(\frac{\partial E^{level,\alpha_i+1}_{\text{recursive-fragment},\alpha_i}(i)}{\partial \mathbf{R}_{\alpha_i}} - \frac{\partial E^{level,\alpha_i}_{\text{recursive-fragment},\alpha_i}(i)}{\partial \mathbf{R}_{\alpha_i}} \right) \frac{\partial \mathbf{R}_{\alpha_i}}{\partial \mathbf{R}} \tag{10}$$

In these sets of equations, $\mathbf{R}$ represents the coordinate variable for the entire system, and $\mathbf{R}_{\alpha_i}$ and $\mathbf{R}_i$ refer to the fragment coordinate variables. Note that $\mathbf{R}_{\alpha_i}$ and $\mathbf{R}_i$ may include link atoms when bonds are broken during fragmentation. [Generally link atoms are chosen as hydrogen atoms, but as shown in ref 11, it is also possible to use other atoms or larger groups of atoms to match electronegativities.] Hence, $\partial \mathbf{R}_{\alpha_i}/\partial \mathbf{R}$ and $\partial \mathbf{R}_i/\partial \mathbf{R}$ are the Jacobian terms required to transform the gradients.[56]

When charges from *level*,0 are included in *level*,1 (electronic embedding, abbreviated hereafter as EE), the gradients above include additional terms due to the change in energy that results from the change in background charge, which, in turn, is dependent on the nuclear positions of the system outside *i*. These are not considered here and will be discussed as part of future publications.

The analytical gradients here allow a direct implementation of Born−Oppenheimer Molecular Dynamics (BOMD).

III. RESULTS AND DISCUSSION

Several different water clusters are used here as benchmark systems. Because of their significance in biological,[72−79] atmospheric,[80−83] and condensed phase chemistry,[84] the protonated water clusters have been extensively studied during the past two decades by both theoretical and experimental communities, and thus are good model systems for the benchmark calculations. The level of experimental and theoretical scrutiny can be gauged from the reference list. Specifically, there has been substantial effort from the electronic structure community,[38,85−92] the classical and quantum dynamics communities,[93−105] and the field of experimental gas-phase spectroscopy.[85,106−113] Furthermore, there have been a variety of polarizable water models in the literature,[66,100,114−125] some of which incorporate the basic ideas behind fragment-based methodologies[53] and others that use many-body expansions.[126] Our reference list is certainly not exhaustive, given the richness of this area of research.

We consider three different protonated water clusters here. We first examine the accuracy of our fragmentation procedure by

DOI: 10.1021/acs.jctc.5b00433
J. Chem. Theory Comput. 2015, 11, 3978−3991

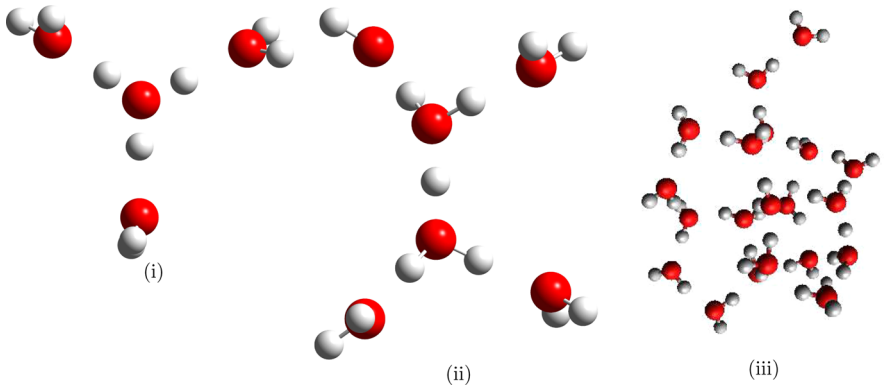

Figure 2. Optimized structure for each of the benchmark systems used in this publication.

comparing energetic results with regular full system calculations at a variety of geometries. Reduced dimensional potential energy surfaces (PES) are computed for this purpose along each normal mode for the $H_9O_4^+$ (or the Eigen system[127]), and four selected normal modes for the protonated 21-water cluster. Given the good accuracy of the energies, we further carried out AIMD simulations on $H_9O_4^+$ and $H_{13}O_6^+$ (the solvated Zundel[128] cation). Energy conservation is analyzed and vibrational density of states are computed from the dynamics trajectories. One optimized structure for each of these three systems is shown in Figure 2.

All computations pertaining to the fragmentation procedure discussed here are performed using a C++ wrapper code that utilizes the Gaussian series of electronic structure programs[129] to compute energy and gradients. The wrapper is modular and may be generalized to other electronic structure platforms. The analysis is performed using a set of shell scripts. The entire suite of programs is available upon request from the corresponding author.

III(A). Fragmentation Algorithm for Water Clusters. Accounting for the hydrogen bonds in water are a critical portion of any fragmentation algorithm, since these have a significant role on the energetic and structural properties of the cluster. To account for all hydrogen bonds, we derive fragments for a given molecular structure, during dynamics, as follows:

(1) Given a minimum oxygen−oxygen separation (D_i) for a chosen oxygen atom, a maximum of three additional water molecules are included inside the solvation sphere of the water molecule represented by O_i, such that the respective oxygen−oxygen distances are within 10% off D_i.

(2) Bonded hydrogen atoms are then included to form primitive fragments. Here, we use two well-known limits for the protonated water cluster system: (a) the Zundel $H_5O_2^+$ system, where the oxygen−oxygen distance is 2.5 Å, on average and the shared proton sits on the middle; and (b) the Eigen $H_9O_4^+$, system, which is most similar to that of H_3O^+, but is fully solvated. To include the definition of delocalized charge as afforded by these two systems, the cutoff for O−H distance is 1.4 Å in all our simulations.

(3) All fragments that include the excess proton inside their envelope have a net charge of +1. The remainder are neutral.

(4) Finally, all fragments that do not contain electrons are excluded from the calculation. See, for example, the intervening proton in Figure 3(ii). This fragment does not contain any electrons. Since the energies computed using electronic structure are interaction energies, a fragment containing just one proton has zero interaction energy. (This definition would need to be modified if molecular mechanics is used at the lower level of theory, which is not the case in this publication.)

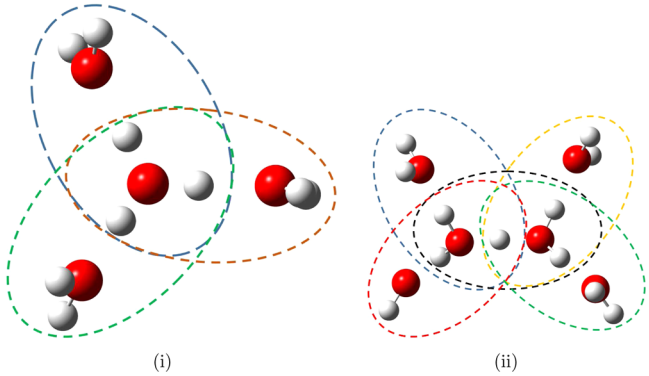

Figure 3. Illustration of the fragmentation procedure. (i) $H_9O_4^+$ is divided into three overlapping primitive fragments denoted by shapes of different color. The central H_3O^+ shared among all primitive fragments is a derivative fragment. (ii) $H_{13}O_6^+$ is partitioned into five primitive fragments, and the multiple overlapping regions across these primitive fragments generate two H_3O^+ derivative fragments. See text for further details.

Primitive fragments generated by this algorithm overlap with adjacent fragments through an intervening hydronium ion or a water molecule. These intersections ensure all hydrogen bonds are equally treated. Two examples are given in Figure 3. Furthermore, based on the above conditions, one might encounter a change in fragment topology during dynamics. These aspects are not treated in the current publication and aspects regarding dynamical fragmentation will be considered in future publications.

III(B). Accuracy of Reduced Dimensional Potential Energy Surfaces. During dynamics, the system may sample a variety of configurations in phase space. Thus, the accuracy of potential surfaces is critical for AIMD and for quantum wavepacket dynamics in order to study reactions and vibrational properties. This is especially true for systems that show a strong tendency for anharmonic behavior. Thus, two protonated water clusters, $H_9O_4^+$ and $H(H_2O)_{21}^+$, are chosen as the benchmark systems here.

To construct reduced dimensional surfaces that can describe collective behavior, we first compute normal-mode vectors from the Hessian matrix obtained at the B3LYP/6-31+g(d,p) level of theory. The reference geometry used for this purpose is a minimum at the noted level of theory. This equilibrium geometry is then perturbed along each of the normal mode coordinates to

DOI: 10.1021/acs.jctc.5b00433
J. Chem. Theory Comput. 2015, 11, 3978−3991

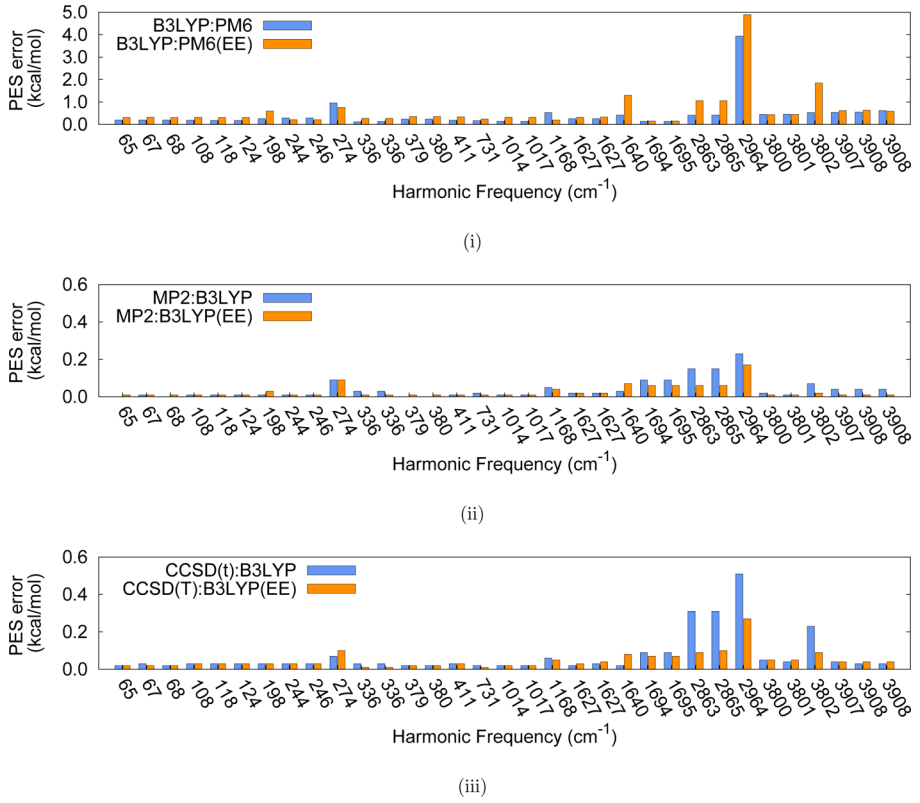

Figure 4. Potential energy surface error as defined in eq 11 for the $H_9O_4^+$ system. All B3LYP, MP2, and CCSD(T) calculations are performed using the 6-31+g(d,p) basis function. The horizontal axis is the same in all cases, because the calculations are performed along the B3LYP normal coordinates.

Table I. Weighted Absolute Error Using ϵ in eq 11 for B3LYP Normal Modes Directions (6-31+g(d,p) Basis Set Is Used for All B3LYP, MP2, and CCSD(T) Calculations)[a]

	Weighted Absolute Error (kcal/mol)					
	B3LYP:PM6		MP2:B3LYP		CCSD(T):B3LYP	
weighting function	PES error[b]	harmonic[c]	PES error[b]	harmonic[c]	PES error[b]	harmonic[c]
w^{u}	0.424		0.040		0.072	
w^{gs}	0.214	7.28	0.008	7.10	0.018	7.09
$w^{Boltzmann}$(100 K)	0.300	23.8	0.026	23.8	0.036	23.8
$w^{Boltzmann}$(200 K)	0.349	43.9	0.033	42.1	0.045	41.3
$w^{Boltzmann}$(300 K)	0.415	62.4	0.039	56.7	0.058	57.8

[a]System: $H_9O_4^+$. [b]This is the average value of ϵ in eq 11 for 33 modes. Hence, it is the net, weighted, mean absolute deviation across 693 nuclear configurations. [c]Same as column on left except that E^i_{frag} in eq 11 is replaced by a harmonic potential with the appropriate force constant. This indicates deviation from the harmonic approximation.

obtain structures to compute one-dimensional potential surfaces. These surfaces are benchmarked for accuracy between the fragmentation procedure described above and a regular full system calculation at the higher level of theory. Deviations from harmonic behavior are also gauged, since these have a critical role in many recent experimental vibrational spectra.[85,98,99,102,103,109−112]

III(B)-1. The Eigen Cation, $H_9O_4^+$. Directions along all 33 normal-mode vectors are investigated. Three combinations of levels of theory are used: (a) B3LYP/6-31+g(d,p):PM6, (b) MP2/6-31+g(d,p):B3LYP/6-31+g(d,p), and (c) CCSD(T)/6-31+g(d,p):B3LYP/6-31+g(d,p). These are compared with full calculations at B3LYP/6-31+g(d,p), MP2/6-31+g(d,p), and CCSD(T)/6-31+g(d,p), respectively. The inclusion of electronic embedding (EE) using Mulliken point charges from the lower level of theory is also tested here. Along each mode, 21 structures are evenly distributed with a collective maximum deviation of 0.5 Å on either side of the optimized structure. A total of 693 structures were probed for each level of theory highlighted above. The mean absolute error (ϵ) between the fragment-based approach and the full calculation performed at the higher level is

$$\epsilon = \sum_{i}^{N_p} \left| (E^i_{frag} - E^{ref}_{frag}) - (E^i_{high} - E^{ref}_{high}) \right| w_i \qquad (11)$$

where N_p is the number of calculations, w_i is a weighting function (see below), E^i_{frag} is the potential energy from the fragment-based calculation for the ith configuration, and E^i_{high} represents the corresponding energy calculated at the higher level of theory. For example, for fragment calculation at CCSD(T)/6-31+g(d,p):B3LYP/6-31+g(d,p), E^i_{high} represents the CCSD(T)/6-31+g(d,p) energy. The quantities E^{ref}_{frag} and E^{ref}_{high} refer to the energy of a reference geometry at the fragment and higher level

DOI: 10.1021/acs.jctc.5b00433
J. Chem. Theory Comput. 2015, 11, 3978−3991

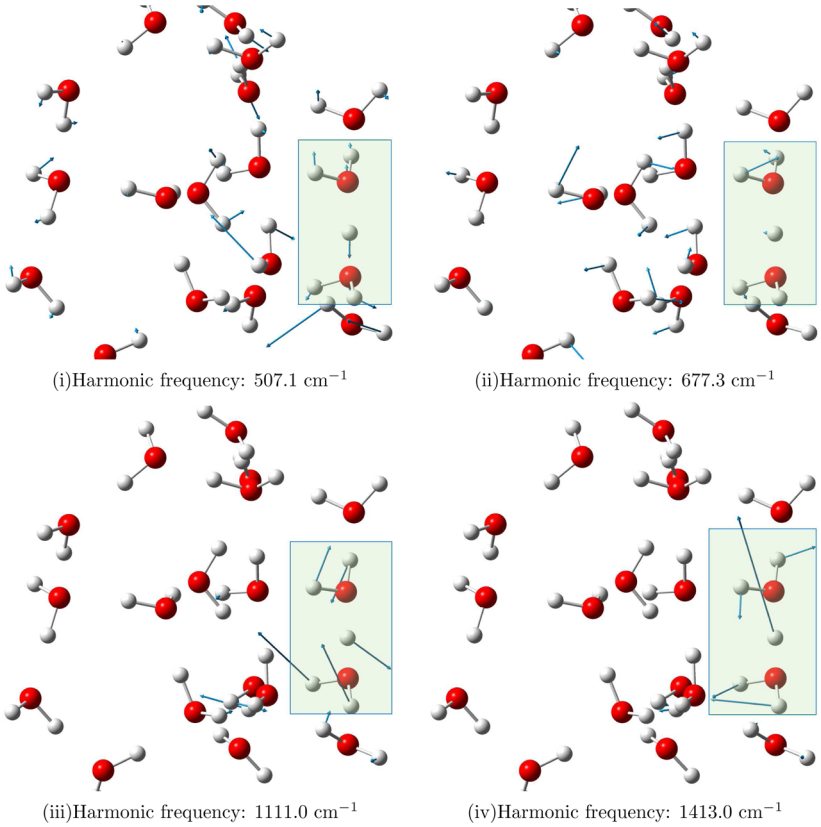

Figure 5. Normal-mode vectors from the optimized protonated 21-water cluster used for potential surface calculations. The modes are chosen to represent the shared proton stretch and bend components of a solvated Zundel substructure (highlighted) within the system.

of theory. In this study, the reference geometry is chosen to be the respective minimum energy conformation across all chosen structures. The error for each mode when using a uniform weighting function, $w_i = 1/21$ and $N_P = 21$, is shown in Figure 4. Results are also presented in Table I for other weight functions, w_i, with the following rationales:

(a) w^u is the uniform weighting function for all nuclear configurations,

(b) w^{gs} represents the choice of ground-state wavepacket as a weighting function. This function is obtained from the set of eigenstates for a one-dimensional Schrödinger equation constructed using the higher-level potential surface (E^i_{high} above). In Table I, errors corresponding to w^{gs} are average values across all 33 normal-mode directions. Evaluating this error has significance in quantum dynamical propagation since the ground-state wavepackets of unperturbed systems are a common choice for initial conditions in dynamics. Furthermore, this is also representative of the "true error" (as compared to rationale (a) above), since the ground state represents sampling of the potential surface under ambient conditions.

(c) $w^{Boltzmann}(T)$ is the Boltzmann factor for the ith grid point at temperature T. It is defined as

$$w^{\text{Boltzmann}}(T) = \frac{e^{-\beta E^i_{\text{high}}}}{\sum_j e^{-\beta E^j_{\text{high}}}}$$

As shown in Figure 4, most of the calculations have a full surface error of <1 kcal/mol when EE is not included within the B3LYP/6-31+g(d,p):PM6 combination. When EE is included, the error uniformly increases, which indicates that charges from PM6 are not a good candidate for EE. In Figure 4(ii), the MP2/6-31+g(d,p):B3LYP/6-31+g(d,p) combination is presented and EE is constructed at the B3LYP level. All modes have a full surface error of <0.3 kcal/mol. Similarly, for Figure 4(iii), the CCSD(T)/6-31+g(d,p):B3LYP/6-31+g(d,p) combination also shows good accuracy. In these cases, it can be seen that EE for most of the modes improves accuracy.

From Table I, under the columns marked "PES error", it is also seen that the mean absolute error over all 693 structures is <0.5 kcal/mol for B3LYP/6-31+g(d,p):PM6, <0.05 kcal/mol for MP2/6-31+g(d,p):B3LYP/6-31+g(d,p), and <0.07 kcal/mol for CCSD(T)/6-31+g(d,p):B3LYP/6-31+g(d,p). Clearly, MP2/6-31+g(d,p): B3LYP/6-31+g(d,p) is quite impressive and will be used for AIMD studies in the next section. (Also see the Supporting Information for a more-detailed exposition of these errors, which includes a comparison of errors with mean absolute deviations of the potential surface at the higher level of theory, and a comparison of errors with the zero point energy obtained from the higher level of theory.) In all cases, the full surface errors, relative to the mean absolute deviations in the surface, are in the range of 0.01%−5.27% for MP2:B3LYP, and 0.04%−10.52% for CCST(T):B3LYP. The singular 10.52% error for CCST(T):B3LYP is due to a shifted surface, whose curvature is the same. Hence, we have also provided potential surface plots for a select set of worst-case scenarios in the Supporting Information. The relative error is larger for B3LYP:PM6, but we have already seen, from Figure 4, that PM6 provides a poor approximation for coupling across fragments. However, as will be seen from the vibrational density of states provided in the next section, the difference in potential surface gets averaged out during dynamics, leading to qualitative similarity between the

DOI: 10.1021/acs.jctc.5b00433
J. Chem. Theory Comput. 2015, 11, 3978−3991

Table II. Weighted Absolute Error Using ϵ in eq 11 for $H(H_2O)_{21}^+$ at Four Selected B3LYP Normal Modes (6-31+g(d,p) Basis Set Is Used for All B3LYP and MP2 Calculations)

		Weighted Absolute Error (kcal/mol)				
		PES Error[a]		Harmonic[b]	PES Error[a]	
mode freq (cm^{-1})		B3LYP:PM6[c]	B3LYP:PM6(EE)[c]	B3LYP	MP2:B3LYP[c]	MP2:B3LYP(EE)[c]
507.1 (Figure 5(i))	w^u	0.08	1.06	8.65	0.03	0.03
	w^{gs}	0.04	0.58	1.34	0.01	0.00
677.3 (Figure 5(ii))	w^u	0.35	1.30	12.84	0.08	0.08
	w^{gs}	0.12	0.61	1.67	0.01	0.01
1111.0 (Figure 5(iii))	w^u	0.21	1.94	34.78	0.11	0.09
	w^{gs}	0.06	0.68	2.81	0.01	0.01
1413.0 (Figure 5(iv))	w^u	0.56	3.09	52.94	0.04	0.04
	w^{gs}	0.13	0.78	3.99	0.01	0.02

[a]This is the average value of ϵ in eq 11. Hence, it is the net, weighted, mean absolute deviation across 21 nuclear configurations chosen along each normal mode. [b]Same as column on left except that E^i_{frag} in eq 11 is replaced by a harmonic potential with the appropriate force constant. This indicates deviation from the harmonic approximation. The optimized geometry in this case is from the B3LYP calculation. [c]Each fragment-based electronic structure calculation contains 28 primitive and 19 derivative fragments. The primitive fragments are either $H_5O_2^+$ or $(H_2O)_2$ and derivatives are H_2O or H_3O^+, as illustrated in Figure 3 for the smaller clusters. The fragmentation topology is computed at the B3LYP optimized geometry.

B3LYP:PM6 density of states and the one calculated from pure B3LYP.

Before we proceed further, we also gauge the performance of the fragment-based methods in capturing the intrinsic anharmonicities in the reduced dimensional surface calculations. This is done by comparing the scanned surfaces with the surfaces obtained using the harmonic approximation. The results are shown in Table I under the columns marked "harmonic". It can be clearly seen that harmonic approximation produces significant error. Even at the zero-point level (that is, using the ground-state wavepacket weighting function), the mean absolute error between the harmonic surface and that obtained from the regular scan is 7.10 kcal/mol. This is a strong evidence for the anharmonicity in these systems and is consistent with several recent studies.[98,99,103] In the Boltzmann weighted case, the error for harmonic approximation increases drastically as the temperature increases. In all cases, the fragmentation approach is found to be quite accurate.

III(B)-2. Protonated 21-Water Cluster, $H(H_2O)_{21}^+$. Fragmentation methods are designed to treat relatively large systems. Hence, we also extend our benchmark to the protonated 21-water cluster. This is an interesting system, since it has been shown in several studies[85,96−99] that conformational sampling and anharmonic effects of the shared proton are critical features that dominate the spectroscopy of the problem. One particular structure obtained from previously conducted AIMD studies[99] is provided in Figure 2(iii). Within the harmonic spectrum for this particular structure, obtained using the B3LYP/6-31g+(d,p) level of theory, we have chosen four normal-mode vectors such that these include the characteristic vibrations of a Zundel substructure solvated within this larger cluster. These modes are shown in Figure 5 and involve the stretch and bend modes of the excess proton within the Zundel substructure. Two combinations of fragment-based theories are used: B3LYP/6-31+g(d,p):PM6 and MP2/6-31+g(d,p):B3LYP/6-31+g(d,p). To compute the potential surfaces along the chosen mode vectors, the structures are perturbed by as much as ±1.0 Å off the optimized structure. Energies for 21 different structures are calculated for each mode within this bracketed region, and the mean absolute error is obtained using w^u and w^{gs}. As shown in Table II, the fragmentation approach is in excellent agreement with the reference calculations, which, in this case, were performed using the MP2 level of theory on the full system. In addition, there is strong deviation from the harmonic approximation and this is to be expected, based on the previous studies listed above. As previously discussed, EE is only useful when the lower level of theory is B3LYP.

III(C). *Ab Initio* Molecular Dynamics Studies Using Fragment-Based Electronic Structure Calculations. In this section, we gauge the utility of the fragmentation procedure by computing classical, BOMD trajectories. We first inspect the energy conservation and then proceed to evaluate the vibrational density of states using the velocity autocorrelation function. Two protonated water clusters are considered here: the Eigen cation, $H_9O_4^+$, and the solvated Zundel cation, $H_{13}O_6^+$. Both of these forms of the protonated species in water have been found to have critical significance in proton transfer in biological and aqueous environments.[84,127,128,130−133] Here, two combinations of fragment-based theories, B3LYP/6-31+g(d,p):PM6 and MP2/6-31+g(d,p):B3LYP/6-31+g(d,p), were tested and benchmarked against full-system BOMD calculations (i.e., without employing the fragmentation technique), at the B3LYP/6-31+g(d,p) and MP2/6-31+g(d,p) levels of theory.

Before we proceed to analyze and compare the dynamics data, it is critical to evaluate the effectiveness of the dynamics procedure. Energy conservation is a critical measure for any propagation scheme. Discontinuities in potential will arise when the topology of the cluster changes during dynamics, which then makes the initial fragmentation assignment invalid. In this paper, as mentioned earlier, our study does not include dynamical fragmentation.[65,66] (An adaptive, conservative, fragmentation scheme is currently under development and will be introduced in a future publication.) We first gauge the smoothness of the potential for the case where no topological changes occur during dynamics and then proceed to probe the effectiveness of the fragmentation technique in obtaining dynamical properties such as correlation functions.

As seen in Table III, the total energies in all the simulations within the given duration are very well-conserved for both fragment-based calculations and full system calculations. The

DOI: 10.1021/acs.jctc.5b00433
J. Chem. Theory Comput. 2015, 11, 3978−3991

Table III. Energy Conservation Properties for the BOMD Simulations

level of theory[a]	duration (ps)[b]	ave temp (K)	ΔE (kcal/mol)[c]
	$H_9O_4^+$ System		
B3LYP	2.0	898.9 ± 180.6	0.016
B3LYP	4.8	153.3 ± 26.3	0.011
MP2	4.8	150.0 ± 28.0	0.002
B3LYP:PM6	2.0	930.1 ± 151.2	0.015
MP2	2.0	928.6 ± 170.5	0.013
MP2:B3LYP	2.0	935.8 ± 163.1	0.030
	$H_{13}O_6^+$ System		
B3LYP	0.8	594.4 ± 104.6	0.017
B3LYP	4.1	150.6 ± 21.8	0.008
MP2	3.4	150.0 ± 22.7	0.008
B3LYP:PM6	0.8	609.7 ± 92.1	0.070
MP2	0.8	604.7 ± 93.6	0.015
MP2:B3LYP	0.8	607.7 ± 90.9	0.020

[a]The 6-31+g(d,p) basis set is used for B3LYP and MP2. [b]A time step of 0.2 fs is used for all simulations. [c]Root-mean-square deviation of the total energy.

short-dynamics time scales are a manifestation of the fact that topological changes do occur, as one might expect. However, the question remains whether dynamical properties are well-represented during these fragmentation calculations, particularly, given the local nature of the problem. Toward this, we compute the vibrational density of states, from dynamics data, using the Fourier transform of velocity autocorrelation (FT-VAC) function:

$$\begin{aligned} I_V(\omega) &= \lim_{T\to\infty} \int_{t=0}^{t=T} \mathrm{d}t\, \exp(-\imath\omega t)\langle \mathbf{V}(0)\cdot\mathbf{V}(t)\rangle \\ &= \lim_{T\to\infty} \sum_{i=1}^{N_{\text{atoms}}} \sum_{j=1}^{3} \int_{t=0}^{t=T} \mathrm{d}t\, \exp(-\imath\omega t) \\ &\quad \times \left[\int_{t'=0}^{t'=T} \mathrm{d}t'\, V_{i,j}(t')V_{i,j}(t'+t)\right] \\ &= \lim_{T\to\infty} \sum_{i=1}^{N_{\text{atoms}}} \sum_{j=1}^{3} \left| \int_{t=0}^{t=T} \mathrm{d}t\, \exp(-\imath\omega t)V_{i,j}(t)\right|^2 \end{aligned} \tag{12}$$

where the term $\langle ... \rangle$, in the first line, indicates the ensemble average and is equal to the t'-integral (enclosed within square-brackets) in the second line, under conditions of ergodicity. The quantity $V_{i,j}(t)$ is the velocity along the jth component for the ith atom. We have used the convolution theorem[134] to reduce the second equation line to the third equation line. It is also important to note that, since time-correlation functions involving nuclear velocities are utilized to obtain vibrational properties, a constant energy simulation with an associated conservative Hamiltonian corresponding to the real system is critical.

Because of anharmonic effects, the vibrational density of states generally is dependent on the amount of thermal energy present in the clusters. These aspects are very well described in a series of *ab initio* dynamics publications[102,135,136] and will not be discussed further here.

The $I_V(\omega)$ results for $H_9O_4^+$ are presented in Figure 6 and those for $H_{13}O_6^+$ are presented in Figure 7. All the major peaks from regular full-system dynamics are reproduced in fragment-based AIMD simulations. Since $I_V(\omega)$ represents the vibrational density of states, it appears that the salient features are faithfully reproduced in the fragment calculations.

While $I_V(\omega)$ provides the vibrational density of states, the Fourier transform of dipoles provides peak intensities proportional to the change in dipole moment of the system and the vibrational spectrum,[98,99,102,136−141] inclusive of these intensities, is computed as

$$\begin{aligned} \alpha_\mu^{\text{QC}}(\omega) &\propto \frac{\omega}{1-\exp(-\beta\hbar\omega)}\left\{\omega[1-\exp(-\beta\hbar\omega)]\right. \\ &\quad \left. \times \lim_{T\to\infty}\int_{t=0}^{t=T} \mathrm{d}t\, \exp(-\imath\omega t)\langle \boldsymbol{\mu}(\mathbf{0})\cdot\boldsymbol{\mu}(\mathbf{t})\rangle\right\} \\ &\propto \omega^2 \lim_{T\to\infty}\sum_{i=1}^{3}\left|\int_{t=0}^{t=T}\mathrm{d}t\, \exp(-\imath\omega t)\mu_i(t)\right|^2 \end{aligned} \tag{13}$$

The terms inside the curly brackets ($\{...\}$) in the first equation above represent the power-normalized absorption cross-section.[137,138] The prefactor, $\omega/[1-\exp(-\beta\hbar\omega)]$, is a quantum-nuclear correction[139−141] that is obtained based on the harmonic approximation. Over a series of publications[82,83,85,98,99,102,103,135,136,142] it has been demonstrated that these correlation functions provide a good estimate to the vibrational spectrum obtained from experimental action spectroscopy. In Figure 8, we present the quantity $\alpha_\mu^{\text{QC}}(\omega)$ from eq 13 for the full simulations, and these are in good agreement with the vibrational spectra presented in ref 84. Future publications will include dynamically averaged spectral studies using fragment methods.

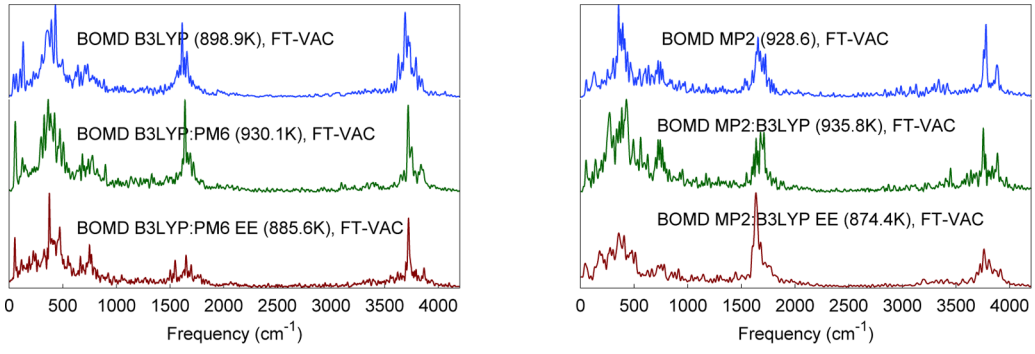

Figure 6. Vibrational density of states for $H_9O_4^+$.

DOI: 10.1021/acs.jctc.5b00433
J. Chem. Theory Comput. 2015, 11, 3978−3991

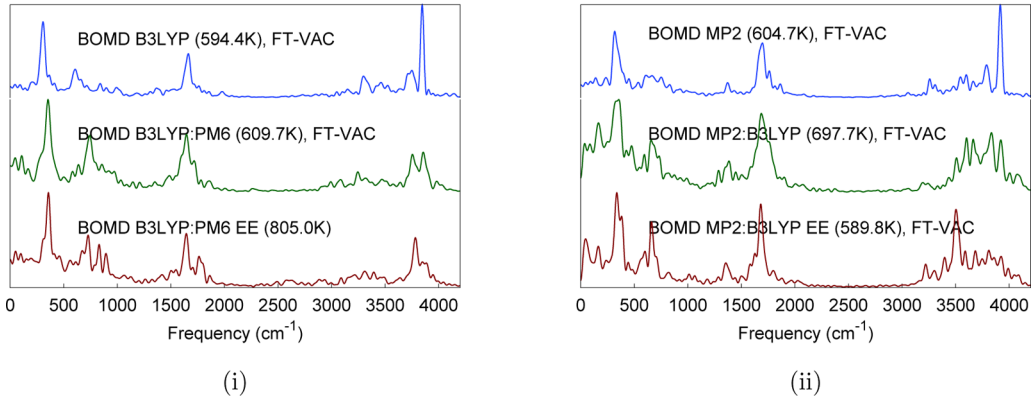

Figure 7. Vibrational density of states of $H_{13}O_6^+$.

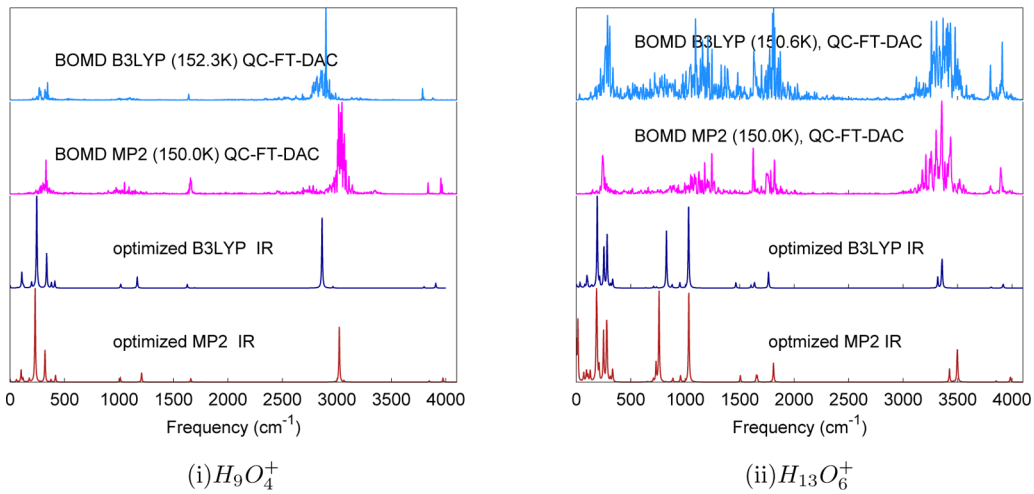

Figure 8. The two top panels in each figure depict the quantity in eq 13 obtained using dynamics simulations. The bottom panels are results from frequency calculations at optimized geometries.

IV. CONCLUDING REMARKS

In this publication, we utilize fragment-based electronic structure calculations to compute *ab initio* molecular dynamics (AIMD) trajectories and reduced dimensional potential energy surfaces. The fragment-based electronic structure protocol is based on the ONIOM formalism but includes overlapping "model" systems. The "model" system intersections are then suitably accounted for using the inclusion−exclusion principle known in set theory.[49] Furthermore, the electronic resolution for each "model" may be recursively refined, and such refinements may also contain overlapping sub-fragments. In this fashion, the electronic structure is resolved in multiple layers and multiple resolutions. Efficiency in fragmentation arises in the current formalism through utilization of a bit-manipulation algorithm, where the fragments are represented as bits in an integer. Our general algorithm is, of course, related strongly to the large body of existing fragment-based technologies. We underline critical overlaps with the molecules-in-molecules (MIM) formalism[42] and the molecular tailoring approach.[37]

The approach is benchmarked for a set of protonated water clusters. These systems have been known to be a challenge for the electronic structure community, as well as the dynamics community,[38,85−105] especially with reference to the large body of cluster spectroscopy results.[84,85,107,108,110,112,113] The challenge in these systems resides in (a) accurate treatment of anharmonicity, and (b) the fact that larger internal energies lead to changes in hydrogen-bonding architectures and subsequent proton hops. Previous studies have indicated that both aspects may be suitably described using AIMD calculations.[82,83,96−99,102,103,135,136] However, these simulations are confounded by the plethora of electronic structure calculations required by the "on-the-fly" procedure. Hence, one goal of the current publication was to gauge whether fragment-based electronic structure theory can be used to improve the computational scenario in such fluxional problems. By comparing velocity correlation functions, we found that our well-defined, energy-conserving, fragment-based dynamics trajectories did indeed reproduce the results in good agreement with the regular AIMD trajectories that use the higher level of theory. However, there are a few limitations in our current study which we briefly highlight below and will be improved in future publications:

(a) While our current study does not include molecular topology changes during dynamics, we find that the fragmentation protocol does allow accurate study of both AIMD and description of potential surfaces. As a result, future publications will include the use of adaptive fragmentation techniques. There are several studies in the literature[65,66] that we can build on to solve this problem. However, it is critical to note that an entire class of problems exists, such as conformational changes in proteins, where this development is not required.

DOI: 10.1021/acs.jctc.5b00433
J. Chem. Theory Comput. 2015, 11, 3978−3991

(b) The computational expense associated with the energy expression in eq 2 is limited by the energy calculation for the full system at the lowest level of theory. Acceleration procedures for this aspect will be discussed in future publications.

(c) The gradients discussed in Subsection II(A) do not include electronic embedding. While short-time-scale trajectories are quite stable, future studies will include embedding forces to improve upon this aspect.

APPENDIX A: ALGORITHM TO GENERATE ALL FRAGMENTS (PRIMITIVE AND DERIVATIVE), USING BIT-MANIPULATION ARITHMETIC

In the fragment-based methodology described here, the intersection between all primitive fragments must be constructed. An efficient algorithm for this exponential scaling problem arises by adopting bitwise operations to generate all combinations of fragments. Here, each fragment in the inclusion-exclusion expression $i \cap j \cap k \cap \cdots$ is represented by a binary bit in an integer. The value of the ith bit in the integer denotes the presence (1) or absence (0) of fragment i in the current molecular configuration. A large integer library may be required, depending on the number of fragments involved and the platform being used for the calculation. One such library is available at https://gmplib.org/. A skeletal bitwise manipulation code is provided in Chart 1, as an algorithm, to obtain all derivative fragments. In this algorithm, the first loop iterates over the number of primitive fragments involved in the current molecular configuration. The inner "while" loop then generates the minimum integer that is greater than I and has same number of binary "1"s as I; this new integer represents the next combination. For example, 0011 represents combination of the first and second primitive fragments, and the next combination generated by the "while" loop is 0101 and represents a combination of the first and third primitive fragments.

Chart 1

ALGORITHM 1: Generating all combinations of primitive fragments

```
loop I ≤ number of primitive fragments
  Integer C = (1 ShiftLeft by i bits) -1;
  while C ≤ (1 ShiftLeft by the number of primitive fragments) -1 do
    save C which represents an i-combination.
    Integer x = C BitAND (-C);
    Integer t = C + x;
    C = t BitOR ((C BitXOR t)/x) ShiftRight 2;
  end while
  I = I + 1;
end loop
```

The composition of primitive and derivative fragments is also depicted using integers in which atoms are represented by binary bits. In such a representation, the intersection between any fragments is merely the binary AND operation of the two corresponding integers. Besides, repeated derivative fragments can be easily discarded and the coefficients can be properly merged.

The use of bitwise operations and bit representations improves algorithmic efficiency.

In practice, based on the chemistry of the molecules and fragmentation scheme, the overlap can be restricted to only between a small numbers of fragments.

ASSOCIATED CONTENT

Supporting Information

The Supporting Information is available free of charge on the ACS Publications website at DOI: 10.1021/acs.jctc.5b00433.

Comparison of potential energy surface errors with mean absolute deviations of the potential surface at the higher level of theory, and comparison of errors with the zero point energy obtained from the higher level of theory (PDF)

AUTHOR INFORMATION

Corresponding Author

*E-mail: iyengar@indiana.edu.

Notes

The authors declare no competing financial interest.

ACKNOWLEDGMENTS

This research is supported by the National Science Foundation (Grant No. NSF CHE-1058949 to S.S.I.).

REFERENCES

(1) Kong, L.; Bischoff, F. A.; Valeev, E. F. Explicitly Correlated R12/F12 Methods for Electronic Structure. *Chem. Rev.* **2012**, *112*, 75.

(2) Lyakh, D. I.; Musiał, M.; Lotrich, V. F.; Bartlett, R. J. Multireference Nature of Chemistry: The Coupled-Cluster View. *Chem. Rev.* **2012**, *112*, 182.

(3) Helgaker, T.; Coriani, S.; Jørgensen, P.; Kristensen, K.; Olsen, J.; Ruud, K. Recent Advances in Wave Function-Based Methods of Molecular-Property Calculations. *Chem. Rev.* **2012**, *112*, 543.

(4) Cohen, A. J.; Mori-Sánchez, P.; Yang, W. Challenges for Density Functional Theory. *Chem. Rev.* **2012**, *112*, 289.

(5) Car, R.; Parrinello, M. Unified Approach for Molecular Dynamics and Density-Functional Theory. *Phys. Rev. Lett.* **1985**, *55*, 2471.

(6) Grossman, J. C.; Schwegler, E.; Draeger, E. W.; Gygi, F.; Galli, G. Towards an Assessment of the Accuracy of Density Functional Theory for First Principles Simulations of Water. *J. Chem. Phys.* **2004**, *120*, 300.

(7) Schlegel, H. B. Exploring Potential Energy Surfaces for Chemical Reactions: An Overview of Some Practical Methods. *J. Comput. Chem.* **2003**, *24*, 1514.

(8) Barnett, R. N.; Landman, U. Born-Oppenheimer Molecular-Dynamics Simulations of Finite Systems—Structure and Dynamics of $(H_2O)_2$. *Phys. Rev. B: Condens. Matter Mater. Phys.* **1993**, *48*, 2081.

(9) Iyengar, S. S.; Jakowski, J. Quantum Wavepacket Ab Initio Molecular Dynamics: An Approach to Study Quantum Dynamics in Large Systems. *J. Chem. Phys.* **2005**, *122*, 114105.

(10) Sumner, I.; Iyengar, S. S. Quantum Wavepacket *Ab Initio* Molecular Dynamics: An Approach for Computing Dynamically Averaged Vibrational Spectra Including Critical Nuclear Quantum Effects. *J. Phys. Chem. A* **2007**, *111*, 10313.

(11) Sumner, I.; Iyengar, S. S. Combining Quantum Wavepacket *Ab Initio* Molecular Dynamics (QWAIMD) with QM/MM and QM/QM Techniques: Implementation Blending ONIOM and Empirical Valence Bond Theory. *J. Chem. Phys.* **2008**, *129*, 054109.

(12) Iyengar, S. S.; Sumner, I.; Jakowski, J. Hydrogen Tunneling in an Enzyme Active Site: A Quantum Wavepacket Dynamical Perspective. *J. Phys. Chem. B* **2008**, *112*, 7601.

(13) Li, X.; Iyengar, S. S. Quantum Wavepacket *Ab Initio* Molecular Dynamics: Generalizations Using an Extended Lagrangian Treatment of Diabatic States Coupled Through Multi-Reference Electronic Structure. *J. Chem. Phys.* **2010**, *133*, 184105.

(14) Li, J.; Li, X.; Iyengar, S. S. Vibrational Properties of Hydrogen Bonded Systems Using the Multi-Reference Generalization to the "On-The-Fly" Electronic Structure Within Quantum Wavepacket *Ab Initio* Molecular Dynamics (QWAIMD). *J. Chem. Theory Comput.* **2014**, *10*, 2265.

DOI: 10.1021/acs.jctc.5b00433
J. Chem. Theory Comput. 2015, 11, 3978−3991

(15) Prociuk, A. H.; Iyengar, S. S. A Multi-Wavelet Treatment of the Quantum Subsystem in Quantum Wavepacket Ab-Initio Molecular Dynamics Through an Hierarchical Partitioning of Momentum Space. *J. Chem. Theory Comput.* **2014**, *10*, 2950.
(16) Warshel, A.; Levitt, M. Theoretical Studies of Enzymic Reactions: Dielectric, Electrostatic and Steric Stabilization of the Carbonium Ion in the Reaction of Lysozyme. *J. Mol. Biol.* **1976**, *103*, 227.
(17) Singh, U. C.; Kollman, P. A. A Combined Ab Initio Quantum Mechanical and Molecular Mechanical Method for Carrying out Simulations on Complex Molecular Systems: Applications to the $CH_3Cl + Cl^-$ Exchange Reaction and Gas Phase Protonation of Polyethers. *J. Comput. Chem.* **1986**, *7*, 718.
(18) Field, C.; Bash, P. A.; Karplus, M. A Combined Quantum Mechanical and Molecular Mechanical Potential for Molecular Dynamics Simulations. *J. Comput. Chem.* **1990**, *11*, 700.
(19) Ferenczy, G. G.; Rivail, J.-L.; Surján, P. R.; Náray-Szabó, G. NDDO Fragment Self-Consistent Field Approximation for Large Electronic Systems. *J. Comput. Chem.* **1992**, *13*, 830.
(20) Gao, J. Hybrid Quantum and Molecular Mechanical Simulations: An Alternative Avenue to Solvent Effects in Organic Chemistry. *Acc. Chem. Res.* **1996**, *29*, 298.
(21) Gao, J.; Amara, P.; Alhambra, C.; Field, M. A Generalized Hybrid Orbital (GHO) Method for the Treatment of Boundary Atoms in Combined QM/MM Calculations. *J. Phys. Chem. A* **1998**, *102*, 4714.
(22) Zhang, Y.; Lee, T.-S.; Yang, W. A Pseudobond Approach to Combining Quantum Mechanical and Molecular Mechanical Methods. *J. Chem. Phys.* **1999**, *110*, 46.
(23) Maseras, F.; Morokuma, K. A New "Ab Initio + Molecular Mechanics" Geometry Optimization Scheme of Equilibrium Structures and Transition States. *J. Comput. Chem.* **1995**, *16*, 1170.
(24) Stanton, R. V.; Hartsough, D. S.; Merz, K. M. An Examination of a Density Functional/Molecular Mechanical Coupled Potential. *J. Comput. Chem.* **1995**, *16*, 113.
(25) Alhambra, C.; Byun, K.; Gao, J. The Geometry of Water in Liquid Water from Hybrid Ab Initio–Monte Carlo and Density Functional–Molecular Dynamics Simulations. In *Combined Quantum Mechanical and Molecular Mechanics Methods*; Gao, J., Thompson, M., Eds.; ACS Symposium Series 712; American ChemicaL Society: Washington, DC, 1998; p 35.
(26) Reuter, N.; Dejaegere, A.; Maigret, B.; Karplus, M. Frontier Bonds in QM/MM Methods: A Comparison of Different Approaches. *J. Phys. Chem. A* **2000**, *104*, 1720.
(27) Murphy, R. B.; Philipp, D. M.; Friesner, R. A. A Mixed Quantum Mechanics/Molecular Mechanics (QM/MM) Method for Large-Scale Modeling of Chemistry in Protein Environments. *J. Comput. Chem.* **2000**, *21*, 1442.
(28) Woo, T. K.; Margl, P. M.; Deng, L.; Ziegler, T. A Combined Car-Parrinello Quantum Mechanical-Molecular Mechanical Implementation of Ab Initio Molecular Dynamics Simulations of Extended Systems. In *Combined Quantum Mechanical and Molecular Mechanics Methods*; Gao, J., Thompson, M., Eds.; ACS Symposium Series 712; American ChemicaL Society: Washington, DC, 1998; p 128.
(29) Laio, A.; VandeVondele, J.; Röthlisberger, U. A Hamiltonian Electrostatic Coupling Scheme for Hybrid Car-Parrinello Molecular Dynamics Simulations. *J. Chem. Phys.* **2002**, *116*, 6941.
(30) Eichinger, M.; Tavan, P.; Hutter, J.; Parrinello, M. A Hybrid Method for Solutes in Complex Solvents: Density Functional Theory Combined with Empirical Force Fields. *J. Chem. Phys.* **1999**, *110*, 10452.
(31) Gordon, M. S.; Freitag, M. A.; Bandyopadhyay, P.; Jensen, J. H.; Kairys, V.; Stevens, W. J. The Effective Fragment Potential Method: A QM-Based MM Approach to Modeling Environmental Effects in Chemistry. *J. Phys. Chem. A* **2001**, *105*, 293.
(32) Zhang, Y.; Lin, H.; Truhlar, D. Self-Consistent Polarization of the Boundary in the Redistributed Charge and Dipole Scheme for Combined Quantum-Mechanical and Molecular-Mechanical Calculations. *J. Chem. Theory Comput.* **2007**, *3*, 1378.
(33) Lin, H.; Truhlar, D. G. QM/MM: What Have We Learned, Where Are We, and Where Do We Go from Here? *Theor. Chem. Acc.* **2007**, *117*, 185.
(34) Toniolo, A.; Granucci, G.; Martinez, T. J. Conical Intersections in Solution: A QM/MM Study Using Floating Occupation Semiempirical Configuration Interaction Wave Functions. *J. Phys. Chem. A* **2003**, *107*, 3822.
(35) Gordon, M. S.; Fedorov, D. G.; Pruitt, S. R.; Slipchenko, L. V. Fragmentation Methods: A Route to Accurate Calculations on Large Systems. *Chem. Rev.* **2012**, *112*, 632.
(36) Zhang, D. W.; Zhang, J. Z. H. Molecular Fractionation with Conjugate Caps for Full Quantum Mechanical Calculation of Protein-molecule Interaction Energy. *J. Chem. Phys.* **2003**, *119*, 3599.
(37) Ganesh, V.; Dongare, R. K.; Balanarayan, P.; Gadre, S. R. Molecular Tailoring Approach for Geometry Optimization of Large Molecules: Energy Evaluation and Parallelization Strategies. *J. Chem. Phys.* **2006**, *125*, 104109.
(38) Xantheas, S. S. *Ab Initio* Studies of Cyclic Water Clusters $(H_2O)_n$, $n = 1–6$. II. Analysis of Many-body Interactions. *J. Chem. Phys.* **1994**, *100*, 7523.
(39) Dahlke, E. E.; Truhlar, D. G. Electrostatically Embedded Many Body Expansion for Large Systems, with Applications to Water Clusters. *J. Chem. Theory Comput.* **2007**, *3*, 46.
(40) Dahlke, E. E.; Truhlar, D. G. Electrostatically Embedded Many Body Expansion for Simulations. *J. Chem. Theory Comput.* **2008**, *4*, 1.
(41) Raghavachari, K.; Saha, A. Accurate Composite and Fragment-Based Quantum Chemical Models for Large Molecules. *Chem. Rev.* **2015**, *115*, 5643.
(42) Mayhall, N. J.; Raghavachari, K. Molecules-in-Molecules: An Extrapolated Fragment-Based Approach for Accurate Calculations on Large Molecules and Materials. *J. Chem. Theory Comput.* **2011**, *7*, 1336.
(43) Mayhall, N. J.; Raghavachari, K. Many-Overlapping-Body (MOB) Expansion: A Generalized Many Body Expansion for Nondisjoint Monomers in Molecular Fragmentation Calculations of Covalent Molecules. *J. Chem. Theory Comput.* **2012**, *8*, 2669.
(44) Jacobson, L. D.; Herbert, J. M. An Efficient, Fragment-Based Electronic Structure Method for Molecular Systems: Self-Consistent Polarization with Perturbative Two-Body Exchange and Dispersion. *J. Chem. Phys.* **2011**, *134*, 094118.
(45) Richard, R. M.; Herbert, J. M. A Generalized Many-Body Expansion and a Unified View of Fragment-Based Methods in Electronic Structure Theory. *J. Chem. Phys.* **2012**, *137*, 064113.
(46) Hirata, S. J. Fast Electron-Correlation Methods for Molecular Crystals: an Application to the α, $\beta(1)$, and $\beta(2)$ Modifications of Solid Formic Acid. *J. Chem. Phys.* **2008**, *129*, 204104.
(47) Kamiya, M.; Hirata, S.; Valiev, M. Fast Electron-Correlation Methods for Molecular Crystals Without Basis Set Superposition Errors. *J. Chem. Phys.* **2008**, *128*, 074103.
(48) Beran, G. J. O.; Hirata, S. Fragment and Localized Orbital Methods in Electronic Structure Theory. *Phys. Chem. Chem. Phys.* **2012**, *14*, 7559.
(49) Li, S.; Li, W.; Ma, J. Generalized Energy-Based Fragmentation Approach and Its Applications to Macromolecules and Molecular Aggregates. *Acc. Chem. Res.* **2014**, *47*, 2712.
(50) Collins, M. A.; Bettens, R. P. A. Energy-Based Molecular Fragmentation Methods. *Chem. Rev.* **2015**, *115*, 5607.
(51) Collins, M. A. Systematic Fragmentation of Large Molecules by Annihilation. *Phys. Chem. Chem. Phys.* **2012**, *14*, 7744.
(52) Le, H.-A.; Tan, H.-J.; Ouyang, J. F.; Bettens, R. P. A. Combined Fragmentation Method: A Simple Method for Fragmentation of Large Molecules. *J. Chem. Theory Comput.* **2012**, *8*, 469.
(53) Han, J.; Mazack, M. J. M.; Zhang, P.; Truhlar, D. G.; Gao, J. Quantum Mechanical Force Field for Water with Explicit Electronic Polarization. *J. Chem. Phys.* **2013**, *139*, 054503.
(54) Chung, L. W.; Hirao, H.; Li, X.; Morokuma, K. The ONIOM Method: Its Foundation and Applications to Metalloenzymes and Photobiology. *Wiley Interdiscip. Rev.: Comput. Mol. Sci.* **2012**, *2*, 327.
(55) Chung, L. W.; Sameera, W. M. C.; Ramozzi, R.; Page, A. J.; Hatanaka, M.; Petrova, G. P.; Harris, T. V.; Li, X.; Ke, Z.; Liu, F.; Li, H.-B.; Ding, L.; Morokuma, K. The ONIOM Method and Its Applications. *Chem. Rev.* **2015**, *115*, 5678.

DOI: 10.1021/acs.jctc.5b00433
J. Chem. Theory Comput. 2015, 11, 3978–3991

(56) Rega, N.; Iyengar, S. S.; Voth, G. A.; Schlegel, H. B.; Vreven, T.; Frisch, M. J. Hybrid Ab-Initio/Empirical Molecular Dynamics: Combining the ONIOM Scheme with the Atom-Centered Density Matrix Propagation (ADMP) Approach. *J. Phys. Chem. B* **2004**, *108*, 4210.
(57) Phatak, P.; Sumner, I.; Iyengar, S. S. Gauging the Flexibility of the Active Site in Soybean Lipoxygenase-1 (SLO-1) Through an Atom-Centered Density Matrix Propagation (ADMP) Treatment That Facilitates the Sampling of Rare Events. *J. Phys. Chem. B* **2012**, *116*, 10145.
(58) Phatak, P.; Venderley, J.; Debrota, J.; Li, J.; Iyengar, S. S. Active Site Dynamical Effects That Facilitate the Hydrogen Transfer Process in Soybean Lipoxygenase-1 (SLO-1): Isotope Effects. *J. Phys. Chem. B* **2015**, *119*, 9532.
(59) Eichinger, M.; Tavan, P.; Hutter, J.; Parrinello, M. A Hybrid Method for Solutes in Complex Solvents: Density Functional Theory Combined with Empirical Force Fields. *J. Chem. Phys.* **1999**, *110*, 10452−10467.
(60) Laio, A.; VandeVondele, J.; Rothlisberger, U. A Hamiltonian Electrostatic Coupling Scheme for Hybrid Car-Parrinello Molecular Dynamics Simulations. *J. Chem. Phys.* **2002**, *116*, 6941.
(61) Iannuzzi, M.; Laio, A.; Parrinello, M. Efficient Exploration of Reactive Potential Energy Surfaces Using Car-Parrinello Molecular Dynamics. *Phys. Rev. Lett.* **2003**, *90*, 238302.
(62) Laio, A.; Parrinello, M. Escaping Free-Energy Minima. *Proc. Natl. Acad. Sci. U. S. A.* **2002**, *99*, 12562.
(63) Brorsen, K. R.; Zahariev, F.; Nakata, H.; Fedorov, D. G.; Gordon, M. S. Analytic Gradient for Density Functional Theory Based on the Fragment Molecular Orbital Method. *J. Chem. Theory Comput.* **2014**, *10*, 5297.
(64) Brorsen, K. R.; Minezawa, N.; Xu, F.; Windus, T. L.; Gordon, M. S. Fragment Molecular Orbital Molecular Dynamics with the Fully Analytic Energy Gradient. *J. Chem. Theory Comput.* **2012**, *8*, 5008.
(65) Komeiji, Y.; Mochizuki, Y.; Nakano, T. Three-Body Expansion and Generalized Dynamic Fragmentation Improve the Fragment Molecular Orbital-Based Molecular Dynamics (FMO-MD). *Chem. Phys. Lett.* **2010**, *484*, 380.
(66) Lange, A. W.; Voth, G. A. Multi-State Approach to Chemical Reactivity in Fragment Based Quantum Chemistry Calculations. *J. Chem. Theory Comput.* **2013**, *9*, 4018.
(67) Björklund, A.; Husfeldt, T.; Koivisto, M. Set Partitioning Via Inclusion−Exclusion. *SIAM J. Comput.* **2009**, *39*, 546.
(68) Bakowies, D.; Thiel, W. Hybrid Models for Combined Quantum Mechanical and Molecular Mechanical Approaches. *J. Phys. Chem.* **1996**, *100*, 10580.
(69) Ramabhadran, R. O.; Raghavachari, K. Theoretical Thermochemistry for Organic Molecules: Development of the Generalized Connectivity-Based Hierarchy. *J. Chem. Theory Comput.* **2011**, *7*, 2094.
(70) Hratchian, H. P.; Parandekar, P. V.; Raghavachari, K.; Frisch, M. J.; Vreven, T. QM:QM Electronic Embedding Using Mulliken Atomic Charges: Energies and Analytic Gradients in an ONIOM Framework. *J. Chem. Phys.* **2008**, *128*, 034107.
(71) Mayhall, N. J.; Raghavachari, K.; Hratchian, H. P. ONIOM-Based QM:QM Electronic Embedding Method Using Lwdin Atomic Charges: Energies and Analytic Gradients. *J. Chem. Phys.* **2010**, *132*, 114107.
(72) Pomes, R.; Roux, B. Structure and Dynamics of a Proton Wire: A Theoretical Study of H+ Translocation Along the Single-File Water Chain in the Gramicidin a Channel. *Biophys. J.* **1996**, *71*, 19.
(73) Pomes, R.; Roux, B. Theoretical Study of H^+ Translocation along a Model Proton Wire. *J. Phys. Chem.* **1996**, *100*, 2519.
(74) Decornez, H.; Drukker, K.; Hammes-Schiffer, S. Solvation and Hydrogen-Bonding Effects on Proton Wires. *J. Phys. Chem. A* **1999**, *103*, 2891.
(75) Brewer, M. L.; Schmitt, U. W.; Voth, G. A. The Formation and Dynamics of Proton Wires in Channel Environments. *Biophys. J.* **2001**, *80*, 1691.
(76) Teeter, M. M. Water Structure of a Hydrophobic Protein at Atomic Resolution: Pentagon Rings of Water Molecules in Crystals of Crambin. *Proc. Natl. Acad. Sci. U. S. A.* **1984**, *81*, 6014.
(77) Neidle, S.; Berman, H. M.; Shieh, H. S. Highly Structured Water Network in Crystals of a Deoxydinucleoside-Drug Complex. *Nature* **1980**, *288*, 129.
(78) Lipscomb, L. A.; Peek, M. E.; Zhou, F. X.; Bertrand, J. A.; VanDerveer, D.; Williams, L. D. Water Ring Structure at Dna Interfaces—Hydration and Dynamics of DNA Anthracycline Complexes. *Biochemistry* **1994**, *33*, 3649.
(79) Tu, C.; Rowlett, R. S.; Tripp, B. C.; Ferry, J. G.; Silverman, D. N. Chemical Rescue of Proton Transfer in Catalysis by Carbonic Anhydrases in the Beta- and Gamma-Class. *Biochemistry* **2002**, *41*, 15429.
(80) McEwan, M. J.; Phillips, L. F. *Chemistry of the Atmosphere*; Wiley: New York, 1975.
(81) Wayne, R. P. *Chemistry of Atmospheres: An Introduction to the Chemistry of the Atmospheres of Earth, the Planets, and Their Satellites*; Clarendon Press: Oxford, U.K., 1991.
(82) Dietrick, S. M.; Pacheco, A. B.; Phatak, P.; Stevens, P. S.; Iyengar, S. S. The Influence of Water on Anharmonicity, Stability and Vibrational Energy Distribution of Hydrogen-Bonded Adducts in Atmospheric Reactions: Case Study of the OH + Isoprene Reaction Intermediate Using *Ab-Initio* Molecular Dynamics. *J. Phys. Chem. A* **2012**, *116*, 399.
(83) Iyengar, S. S. Dynamical Effects on Vibrational and Electronic Spectra of Hydroperoxyl Radical Water Clusters. *J. Chem. Phys.* **2005**, *123*, 084310.
(84) Fournier, J. A.; Wolke, C. T.; Johnson, M. A.; Odbadrakh, T. T.; ; Jordan, K. D.; Kathmann, S. M.; Xantheas, S. S. Snapshots of Proton Accommodation at a Microscopic Water Surface: Understanding the Vibrational Spectral Signatures of the Charge Defect in Cryogenically Cooled $H^+(H_2O)_{n=2-28}$ Clusters. *J. Phys. Chem. A* **2015**, DOI: 10.1021/acs.jpca.5b04355.
(85) Shin, J.-W.; Hammer, N. I.; Diken, E. G.; Johnson, M. A.; Walters, R. S.; Jaeger, T. D.; Duncan, M. A.; Christie, R. A.; Jordan, K. D. Infrared Signature of Structures Associated with the $H^+(H_2O)_n$ (n = 6 to 27) Clusters. *Science* **2004**, *304*, 1137.
(86) Vendrell, O.; Gatti, F.; Meyer, H.-D. Dynamics and Infrared Spectroscopy of the Protonated Water Dimer. *Angew. Chem., Int. Ed.* **2007**, *46*, 6918.
(87) Xie, Y.; Remington, R. B.; Schaefer, H. F., III. The Protonated Water Dimer: Extensive Theoretical Studies of $H_5O_2^+$. *J. Chem. Phys.* **1994**, *101*, 4878.
(88) Sadhukhan, S.; Munoz, D.; Adamo, C.; Scuseria, G. E. Predicting Proton Transfer Barriers with Density Functional Methods. *Chem. Phys. Lett.* **1999**, *306*, 83.
(89) Tsai, C. J.; Jordan, K. D. Theoretical Study of the $(H_2O)_6$ Cluster. *Chem. Phys. Lett.* **1993**, *213*, 181.
(90) Xantheas, S. S. *Ab Initio* Studies of Cyclic Water Clusters $(H_2O)_n$, n = 1−6. III. Comparison of Density Functional with MP2 Results. *J. Chem. Phys.* **1995**, *102*, 4505.
(91) Kryachko, E. S. Ab Initio Studies of the Conformations of Water Hexamer: Modelling the Penta-Coordinated Hydrogen-Bonded Pattern in Liquid Water. *Chem. Phys. Lett.* **1999**, *314*, 353.
(92) Hodges, M. P.; Wales, D. J. Global Minima of Protonated Water Clusters. *Chem. Phys. Lett.* **2000**, *324*, 279.
(93) Cheng, H.-P. Water Clusters: Fascinating Hydrogen-Bonding Networks, Solvation Shell Structures, and Proton Motion. *J. Phys. Chem. A* **1998**, *102*, 6201.
(94) Sadeghi, R. R.; Cheng, H.-P. The Dynamics of Proton Transfer in a Water Chain. *J. Chem. Phys.* **1999**, *111*, 2086.
(95) Cheng, H.-P.; Krause, J. L. The Dynamics of Proton Transfer in $H_5O_2^+$. *J. Chem. Phys.* **1997**, *107*, 8461.
(96) Wu, C.-C.; Lin, C.-K.; Chang, H.-C.; Jiang, J.-C.; Kuo, J.-L.; Klein, M. L. Protonated Clathrate Cages Enclosing Neutral Water Molecules: $H^+(H_2O)_{21}$ and $H^+(H_2O)_{28}$. *J. Chem. Phys.* **2005**, *122*, 074315.
(97) Yu, H. B.; Cui, Q. The Vibrational Spectra of Protonated Water Clusters: A Benchmark for Self-Consistent-Charge Density-Functional Tight Binding. *J. Chem. Phys.* **2007**, *127*, 234504.
(98) Iyengar, S. S.; Petersen, M. K.; Day, T. J. F.; Burnham, C. J.; Teige, V. E.; Voth, G. A. The Properties of Ion-Water Clusters. I. the Protonated 21-Water Cluster. *J. Chem. Phys.* **2005**, *123*, 084309.

DOI: 10.1021/acs.jctc.5b00433
J. Chem. Theory Comput. 2015, 11, 3978−3991

(99) Iyengar, S. S. Further Analysis of the Dynamically Averaged Vibrational Spectrum for the "Magic" Protonated 21-Water Cluster. *J. Chem. Phys.* **2007**, *126*, 216101.
(100) Petersen, M. K.; Iyengar, S. S.; Day, T. J. F.; Voth, G. A. The Hydrated Proton at the Water Liquid/Vapor Interface. *J. Phys. Chem. B* **2004**, *108*, 14804.
(101) Iyengar, S. S.; Day, T. J. F.; Voth, G. A. On the Amphiphilic Behavior of the Hydrated Proton: An *Ab Initio* Molecular Dynamics Study. *Int. J. Mass Spectrom.* **2005**, *241*, 197.
(102) Li, X.; Teige, V. E.; Iyengar, S. S. Can the Four-Coordinated, Penta-Valent Oxygen in Hydroxide Water Clusters Be Detected Through Experimental Vibrational Spectroscopy? *J. Phys. Chem. A* **2007**, *111*, 4815.
(103) Dietrick, S. M.; Iyengar, S. S. Constructing Periodic Phase Space Orbits from *Ab Initio* Molecular Dynamics Trajectories to Analyze Vibrational Spectra: Case Study of the Zundel ($H_5O_2^+$) Cation. *J. Chem. Theory Comput.* **2012**, *8*, 4876.
(104) Wei, D.; Salahub, D. R. Hydrated Proton Clusters: *Ab Initio* Molecular Dynamics Simulation and Simulated Annealing. *J. Chem. Phys.* **1997**, *106*, 6086.
(105) Kaledin, M.; Kaledin, A. L.; Bowman, J. M. Vibrational Analysis of the $H_5O_2^+$ Infrared Spectrum Using Molecular and Driven Molecular Dynamics. *J. Phys. Chem. A* **2006**, *110*, 2933.
(106) Okumura, M.; Yeh, L. I.; Myers, J. D.; Lee, Y. T. Infrared Spectra of the Solvated Hydronium Ion: Vibrational Predissociation Spectroscopy of Mass-Selected $H_3O^+(H_2O)_nH_2$. *J. Phys. Chem.* **1990**, *94*, 3416.
(107) Miyazaki, M.; Fujii, A.; Ebata, T.; Mikami, N. Infrared Spectroscopic Evidence for Protonated Water Clusters Forming Nanoscale Cages. *Science* **2004**, *304*, 1134.
(108) Douberly, G. E.; Ricks, A. M.; Duncan, M. A. Infrared Spectroscopy of Perdeuterated Protonated Water Clusters in the Vicinity of the Clathrate Cage. *J. Phys. Chem. A* **2009**, *113*, 8449.
(109) Headrick, J. M.; Diken, E. G.; Walters, R. S.; Hammer, N. I.; Christie, R. A.; Cui, J.; Myshakin, E. M.; Duncan, M. A.; Johnson, M. A.; Jordan, K. Spectral Signatures of Hydrated Proton Vibrations in Water Clusters. *Science* **2005**, *308*, 1765.
(110) Hammer, N. I.; Diken, E. G.; Roscioli, J. R.; Johnson, M. A.; Myshakin, E. M.; Jordan, K. D.; McCoy, A. B.; Huang, X.; Bowman, J. M.; Carter, S. The vibrational predissociation spectra of the $H_5O_2^+ \cdot RG_n$ (RG = Ar,Ne) clusters: Correlation of the solvent perturbations in the free OH and shared proton transitions of the Zundel ion. *J. Chem. Phys.* **2005**, *122*, 244301.
(111) Diken, E. G.; Headrick, J. M.; Roscioli, J. R.; Bopp, J. C.; Johnson, M. A.; McCoy, A. B. Fundamental Excitations of the Shared Proton in the $H_3O_2^-$ and $H_5O_2^+$ Complexes. *J. Phys. Chem. A* **2005**, *109*, 1487.
(112) Asmis, K. R.; Pivonka, N. L.; Santambrogio, G.; Brümmer, M.; Kaposta, C.; Neumark, D. M.; Wöste, L. Gas-Phase Infrared Spectrum of the Protonated Water Dimer. *Science* **2003**, *299*, 1375.
(113) Fridgen, T. D.; MacAleese, P.; Maitre, L.; McMahon, T. B.; Boissel, P.; Lemaire, J. Infrared Spectra of Homogeneous and Heterogeneous Proton-Bound Dimers in the Gas Phase. *Phys. Chem. Chem. Phys.* **2005**, *7*, 2747.
(114) Rick, S. W.; Stuart, S. J.; Bader, J. S.; Berne, B. J. Fluctuating Charge Force Fields for Aqueous Solutions. *J. Mol. Liq.* **1995**, *65-66*, 31.
(115) Schmitt, U. W.; Voth, G. A. Multistate Empirical Valence Bond Model for Proton Transport in Water. *J. Phys. Chem. B* **1998**, *102*, 5547.
(116) Schmitt, U. W.; Voth, G. A. The Computer Simulation of Proton Transport in Water. *J. Chem. Phys.* **1999**, *111*, 9361.
(117) Day, T. J. F.; Soudackov, A. V.; Cuma, M.; Schmitt, U. W.; Voth, G. A. A Second Generation Multi-State Empirical Valence Bond Model for Proton Transport in Aqueous Systems. *J. Chem. Phys.* **2002**, *117*, 5839.
(118) Wang, F.; Voth, G. A. A Linear-Scaling Self-Consistent Generalization of the Multistate Empirical Valence Bond Method for Multiple Excess Protons in Aqueous Systems. *J. Chem. Phys.* **2005**, *122*, 144105.
(119) Brewer, M. L.; Schmitt, U. W.; Voth, G. A. The Formation and Dynamics of Proton Wires in Channel Environments. *Biophys. J.* **2001**, *80*, 1691.
(120) Smondyrev, A. M.; Voth, G. A. Molecular Dynamics Simulation of Proton Transport Near the Surface of a Phospholipid Membrane. *Biophys. J.* **2002**, *82*, 1460.
(121) Smondyrev, A. M.; Voth, G. A. A Novel Method for Structure-Based Predictions of Ion Channel Conductance Properties. *Biophys. J.* **2002**, *83*, 1987.
(122) Wu, Y.; Voth, G. A. Computer Simulation of Proton Transport in Biomolecular Systems. *Biophys. J.* **2003**, *85*, 864.
(123) Voth, G. A. The Computer Simulation of Proton Transport in Biomolecular Systems. *Front. Biosci., Landmark Ed.* **2003**, *8*, s1384.
(124) Ilan, B.; Tajkhorshid, E.; Schulten, K.; Voth, G. A. The Mechanism of Proton Exclusion in Aquaporin Channels. *Proteins: Struct., Funct., Genet.* **2004**, *55*, 223.
(125) Lapid, H.; Agmon, N.; Petersen, M. K.; Voth, G. A. A Bond-Order Analysis of the Mechanism for Hydrated Proton Mobility in Liquid Water. *J. Chem. Phys.* **2005**, *122*, 014506.
(126) Burnham, C. J.; Xantheas, S. S. Development of Transferable Interaction Models for Water. IV. a Flexible, All-Atom Polarizable Potential (TTM2-F) Based on Geometry Dependent Charges Derived from an Ab Initio Monomer Dipole Moment Surface. *J. Chem. Phys.* **2002**, *116*, 5115.
(127) Eigen, M.; de Maeyer, L. Self-Dissociation and Protonic Charge Transport in Water and Ice. *Proc. R. Soc. London, Ser. A* **1958**, *247*, 505.
(128) Zundel, G. In *The Hydrogen Bond-Recent Developments in Theory and Experiments. II. Structure and Spectroscopy*; Schuster, P., Zundel, G., Sandorfy, C., Eds.; North-Holland: Amsterdam, 1976; p 683.
(129) Frisch, M. J.; Trucks, G. W.; Schlegel, H. B.; Scuseria, G. E.; Robb, M. A.; Cheeseman, J. R.; Scalmani, G.; Barone, V.; Mennucci, B.; Petersson, G. A.; Nakatsuji, H.; Caricato, M.; Li, X.; Hratchian, H. P.; Izmaylov, A. F.; Bloino, J.; Zheng, G.; Sonnenberg, J. L.; Hada, M.; Ehara, M.; Toyota, K.; Fukuda, R.; Hasegawa, J.; Ishida, M.; Nakajima, T.; Honda, Y.; Kitao, O.; Nakai, H.; Vreven, T.; Montgomery, J. A.Jr.; Peralta, J. E.; Ogliaro, F.; Bearpark, M.; Heyd, J. J.; Brothers, E.; Kudin, K. N.; Staroverov, V. N.; Keith, T.; Kobayashi, R.; Normand, J.; Raghavachari, K.; Rendell, A.; Burant, J. C.; Iyengar, S. S.; Tomasi, J.; Cossi, M.; Rega, N.; Millam, J. M.; Klene, M.; Knox, J. E.; Cross, J. B.; Bakken, V.; Adamo, C.; Jaramillo, J.; Gomperts, R.; Stratmann, R. E.; Yazyev, O.; Austin, A. J.; Cammi, R.; Pomelli, C.; Ochterski, J. W.; Martin, R. L.; Morokuma, K.; Zakrzewski, V. G.; Voth, G. A.; Salvador, P.; Dannenberg, J. J.; Dapprich, S.; Parandekar, P. V.; Mayhall, N. J.; Daniels, A. D.; Farkas, O.; Foresman, J. B.; Ortiz, J. V.; Cioslowski, J.; Fox, D. J. Gaussian Development Version, Revision H.37+; Gaussian, Inc.: Wallingford CT, 2010.
(130) Agmon, N. The Grotthuss Mechanism. *Chem. Phys. Lett.* **1995**, *244*, 456.
(131) Bell, R. P. *The Proton in Chemistry*; Cornell University Press: Ithaca, NY, 1973.
(132) Eigen, M. Proton Transfer, Acid-Base Catalysis, and Enzymatic Hydrolysis. Part I: Elementary Processes. *Angew. Chem., Int. Ed. Engl.* **1964**, *3*, 1.
(133) Eisenberg, D.; Kauzman, W. *The Structure and Properties of Water*; Oxford University Press: Oxford, U.K., 1969.
(134) Press, W. H.; Teukolsky, S. A.; Vetterling, W. T.; Flannery, B. P. *Numerical Recipes in C*; Cambridge University Press: New York, 1992.
(135) Li, X.; Moore, D. T.; Iyengar, S. S. Insights from First Principles Molecular Dynamics Studies Towards Infra-Red Multiple-Photon and Single-Photon Action Spectroscopy: Case Study of the Proton-Bound Di-Methyl Ether Dimer. *J. Chem. Phys.* **2008**, *128*, 184308.
(136) Li, X.; Oomens, J.; Eyler, J. R.; Moore, D. T.; Iyengar, S. S. Isotope Dependent, Temperature Regulated, Energy Repartitioning in a Low-Barrier, Short-Strong Hydrogen Bonded Cluster. *J. Chem. Phys.* **2010**, *132*, 244301.
(137) Gordon, R. G. Correlation Functions for Molecular Motion. *Adv. Magn. Reson.* **1968**, *3*, 1.
(138) McQuarrie, D. A. *Statistical Mechanics*; University Science Books, Sausalito, CA, 2000.
(139) Berens, P. H.; White, S. R.; Wilson, K. R. Molecular Dynamics and Spectra. II. Diatomic Raman. *J. Chem. Phys.* **1981**, *75*, 515.

DOI: 10.1021/acs.jctc.5b00433
J. Chem. Theory Comput. 2015, 11, 3978−3991

(140) Bader, J. S.; Berne, B. J. Quantum and Classical Relaxation Rates from Classical Simulations. *J. Chem. Phys.* **1994**, *100*, 8359.
(141) Lawrence, C. P.; Nakayama, A.; Makri, N.; Skinner, J. L. Quantum Dynamics in Simple Fluids. *J. Chem. Phys.* **2004**, *120*, 6621.
(142) Pacheco, A. B.; Dietrick, S. M.; Stevens, P. S.; Iyengar, S. S. Pump-Probe" Atom-Centered Density Matrix Propagation Studies to Gauge Anharmonicity and Energy Repartitioning in Atmospheric Reactive Adducts: Case Study of the OH + Isoprene and OH + Butadiene Reaction Intermediates. *J. Phys. Chem. A* **2012**, *116*, 4108.

DOI: 10.1021/acs.jctc.5b00433
J. Chem. Theory Comput. 2015, 11, 3978−3991